ACS NANO

www.acsnano.org

ARTICLE

Robust, Scalable Microfluidic Manufacturing of RNA–Lipid Nanoparticles Using Immobilized Antifouling Lubricant Coating

Yoon-Ho Hwang, Sarah J. Shepherd, Dongyoon Kim, Alvin J. Mukalel, Michael J. Mitchell, David A. Issadore,* and Daeyeon Lee*

Cite This: *ACS Nano* 2025, 19, 1090–1102

Read Online

ACCESS | Metrics & More | Article Recommendations | Supporting Information

ABSTRACT: Despite the numerous advantages demonstrated by microfluidic mixing for RNA-loaded lipid nanoparticle (RNA-LNP) production over bulk methods, such as precise size control, homogeneous distributions, higher encapsulation efficiencies, and improved reproducibility, their translation from research to commercial manufacturing remains elusive. A persistent challenge hindering the adoption of microfluidics for LNP production is the fouling of device surfaces during prolonged operation, which significantly diminishes performance and reliability. The complexity of LNP constituents, including lipids, cholesterol, RNA, and solvent mixtures, makes it difficult to find a single coating that can prevent fouling. To address this challenge, we propose using an immobilized liquid lubricant layer of perfluorodecalin (PFD) to create an antifouling surface that can repel the multiple LNP constituents. We apply this technology to a staggered herringbone microfluidic (SHM) mixing chip and achieve >3 h of stable operation, a >15× increase relative to gold standard approaches. We also demonstrate the compatibility of this approach with a parallelized microfluidic platform that incorporates 256 SHM mixers, with which we demonstrate scale up, stable production at L/h production rates suitable for commercial scale applications. We verify that the LNPs produced on our chip match both the physiochemical properties and performance for both *in vitro* and *in vivo* mRNA delivery as those made on chips without the coating. By suppressing surface fouling with an immobilized liquid lubricant layer, this technology not only enhances RNA-LNP production but also promises to transform the microfluidic manufacturing of diverse materials, ensuring more reliable and robust processes.

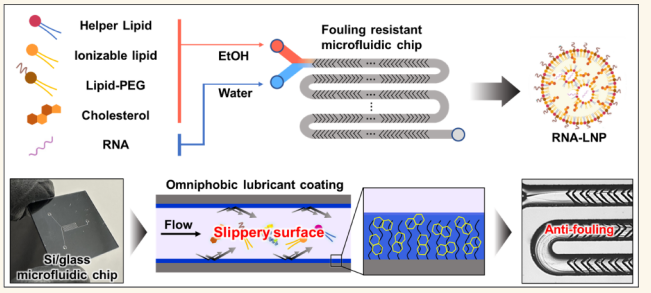

KEYWORDS: *omniphobic coating, nanoprecipitation, staggered herringbone microfluidic mixer, parallelization, vaccine*

INTRODUCTION

Lipid nanoparticles (LNPs) have emerged as highly effective delivery vehicle for mRNA vaccines and therapeutics.[1−3] They played a pivotal role in the Pfizer/BioNTech and Moderna COVID-19 vaccines[4−6] and are now revolutionizing the pharmaceutical industry as they offer opportunities for protein replacement therapies,[7,8] gene editing,[9,10] and accelerated vaccine development.[11,12] RNA-loaded LNP (RNA-LNP) therapeutics are typically composed of an RNA, an ionizable lipid, phospholipid, cholesterol, and a polyethylene glycol−lipid conjugate (PEG−lipid); the ionizable lipid is designed to be neutrally charged at physiological pH and charged when endocytosed so it can release its RNA cargo.[8,11,13] As the field rapidly advances, there is increasing recognition of the profound influence of the choice of the constituent materials of the LNP, as well as its size, charge, and morphology, on its function *in vivo*.[13−16] The function of the LNP *in vivo* is itself also multidimensional, including its tropism to particular cell types or tissues, the immune response it elicits, its ability to induce the target cells to express the protein of interest, and its ability to traverse biological barriers such as the blood−brain barrier.[1,14,17] Given the pivotal role of formulation on LNP function, a critical challenge hindering the successful development of RNA-LNP drugs is the current lack of technologies that can produce a precisely defined LNP formulation across

Received: September 14, 2024
Revised: November 28, 2024
Accepted: December 9, 2024
Published: December 19, 2024

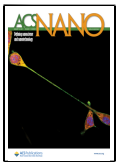

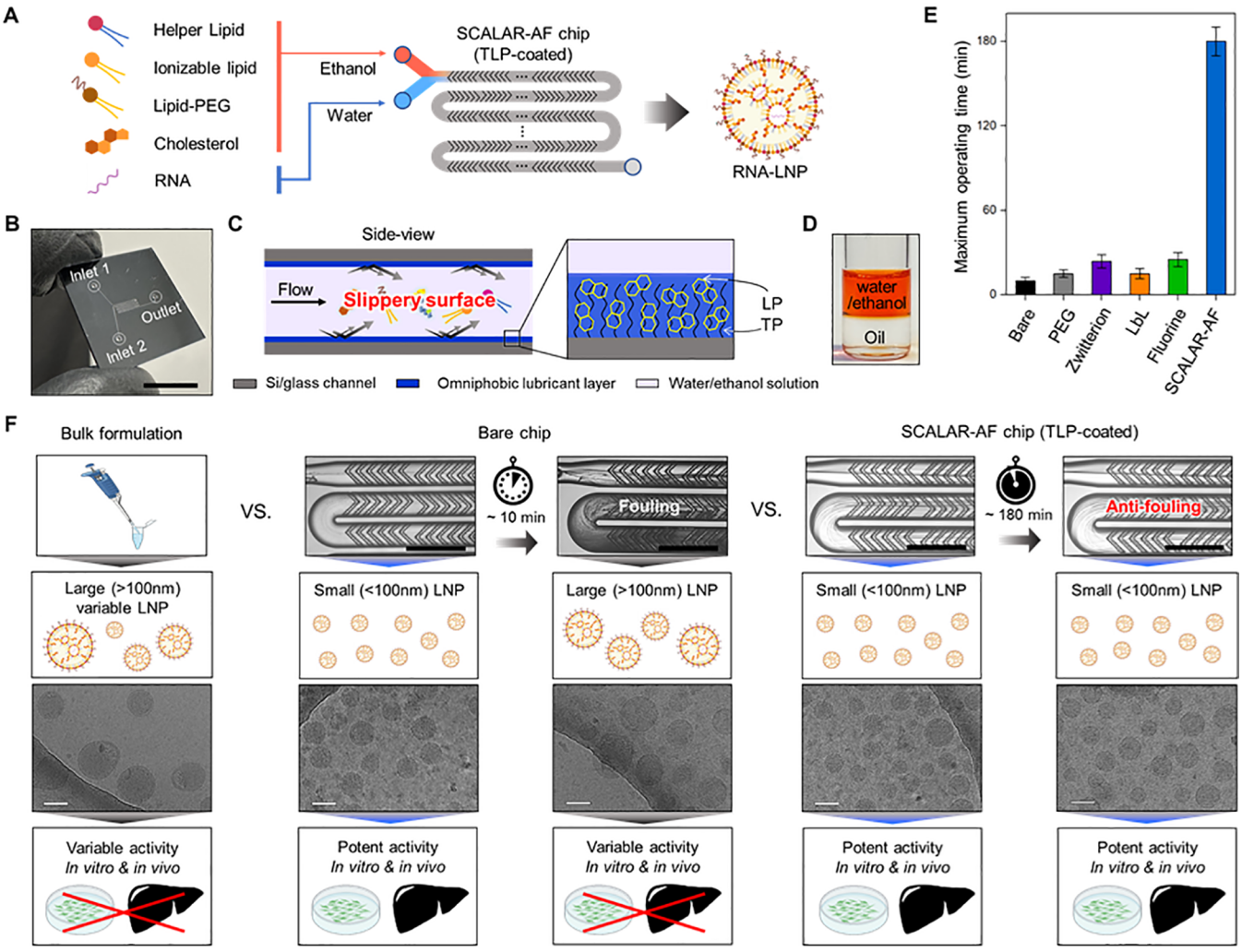

Figure 1. (A) Schematic for robust manufacturing of RNA-LNP using the SCALAR-AF chip. (B) Photograph of the SCALAR-AF chip with a staggered herringbone micromixer. Scale bar: 10 mm. (C) Schematic of the antifouling behavior of RNA-LNP on the lubricant layer-coated surface showing tethered perfluorocarbon (TP) bound to a substrate, which then allows a stable film of liquid perfluorodecalin (LP) to adhere to the surface. (D) Photograph showing the immiscibility between a water/ethanol (3:1) mixture solution and the lubricant oil phase. (E) A plot showing the maximum operating time of microfluidic mixing chips coated with different types of surface treatments. (F) Schematic and microscope images showing the fouling resistant microfluidic chip producing smaller and more homogeneous LNPs for potent RNA delivery, whereas larger and more heterogeneous LNPs are being produced by bulk formulation and conventional microfluidic chips, resulting in imprecise and unreliable delivery of RNA due to fouling inside devices. Scale bar: 300 μm. Cryogenic (cryo)-TEM images showing RNA-LNPs produced by bulk formulation, a bare chip, and a lubricant layer-coated chip before and after fouling. Scale bar: 100 nm.

the many orders of magnitude of throughput—from discovery (mL/h) all of the way to commercial manufacturing (L/h)—all while also meeting the stringent quality standards of the pharmaceutical industry.[7,18,19]

Microfluidics has recently emerged as a promising solution to this problem. Microfluidic mixing units for RNA-LNP production, which allow rapid mixing at the micrometer-scale level, have demonstrated superiority over bulk methods as they provide improved precision for controlling particle size, homogeneity of particle size distributions, morphology, encapsulation efficiencies, and reproducibility.[20−22] Due to the nonuniformity of mixing over the time-scales of LNP formation, the conventional bulk mixing approaches tend to result in poor encapsulation efficiency, high polydispersity, and high batch-to-batch variations.[18,19,21,24] The parallelization of microfluidic mixing units, where ∼1 to >10^4 units can be incorporated onto a single chip and operated in parallel, has successfully demonstrated scale-invariant, precision production of RNA-LNPs.[18,23,24] These devices have been implemented using replica-molding of polymers, 3D printing for rapid prototyping, and silicon and glass (Si/glass). The Si/glass platform is particularly well suited for pharmaceutical manufacturing because of its solvent compatibility and the ability to operate at high pressures.[18,25−27] However, despite the advantages offered by microfluidic mixing units in LNP production, a significant challenge arises from the fouling of RNA-LNP constituents on the surface of the microfluidic device during operation. Over time such a phenomenon significantly degrades the performance of the device through the loss of particle homogeneity and a significant reduction in encapsulation efficiency; moreover, fouling ultimately induces the catastrophic failure of the device due to clogging.[27−29] The inability to effectively prevent fouling in these devices likely impedes the widespread adoption of continuous manufacturing using microfluidic technologies.[19,30,31] In our previous work, we demonstrated that microfluidic chips could be reused or

https://doi.org/10.1021/acsnano.4c12965
ACS Nano 2025, 19, 1090−1102

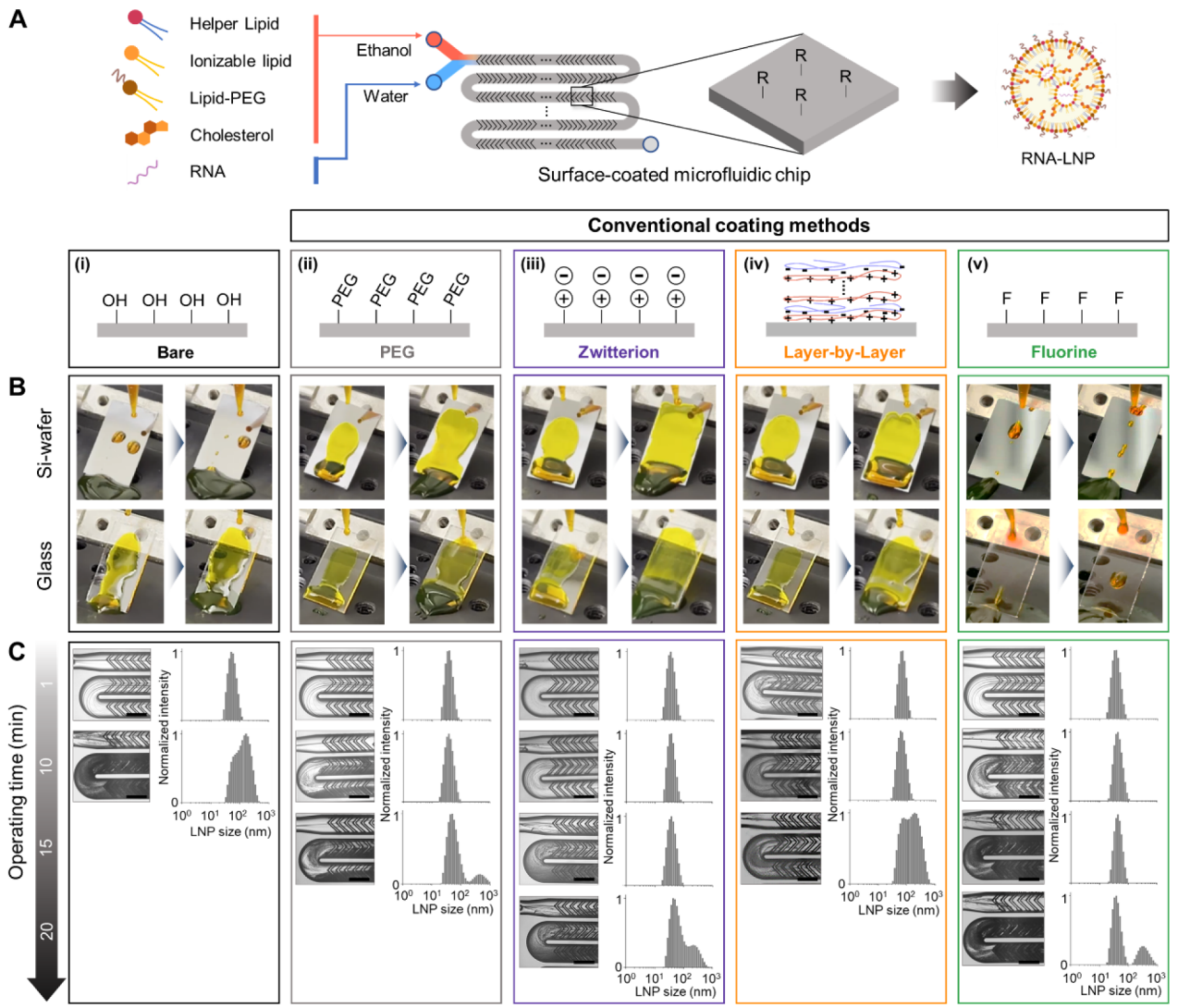

Figure 2. (A) Schematics showing various surface coating methods tested for antifouling behavior in a microfluidic chip for the manufacturing of RNA-LNPs; (i) bare, (ii) PEG, (iii) zwitterion, (iv) layer-by-layer, and (v) fluorine coatings on Si and glass substrates (from left to right). Conventional microfluidic coating strategy fails to protect surface from fouling for LNP formulation. (B) Photographic images showing the wetting/nonwetting of a water/ethanol (3:1) mixture solution on Si-wafer (upper) and glass (bottom) substrates with various coatings at a tilt angle of 45°. (C) Photographs (left columns) and DLS results (right columns) showing the fouling behavior and size variation of the resulting RNA-LNP from each chip as a function of the operation time. Scaling bar: 150 μm.

continuously recycled by applying a cleaning solution to periodically reset it.[25] However, this approach complicates external instrumentation, reduces throughput, and restricts the applicability to batch processing rather than continuous processing. Previous approaches to prevent fouling in microfluidic devices employ surface modifications such as polyethylene glycol (PEG) coating,[32,33] zwitterionic coating,[34,35] layer-by-layer (LbL) coating,[28,36] and amine-/hydroxy-/fluorine-based coating.[37,38] However, these methods were primarily designed to prevent biomolecule adsorption in aqueous environments and have not been successfully applied to the RNA-LNP manufacturing process, which involves solvent mixtures of water/ethanol for precipitation and self-assembly.

Here, we address this challenge by developing a microfluidic chip that incorporates a lubricant oil layer coating to inhibit fouling, enabling continuous and robust manufacturing of RNA-LNPs (Figure 1). Our microfluidic mixing chip, termed SCALAR-AF (silicon scalable lipid nanoparticle generation−anti fouling platform), is entirely fabricated with silicon and glass (Si/glass) substrates to meet the manufacturing requirements of the pharmaceutical industry (Figure 1B).[25] When the Si/glass chip's channels are uncoated, fouling occurs within 10 min into the production of RNA-LNPs, a phenomenon also observed with polydimethylsiloxane (PDMS) and other polymer microfluidic chips (Figures S1 and 1E). We evaluate various gold standard strategies to prevent fouling, including coating with PEG, zwitterion, LbL, and fluorine coatings; however, fouling occurred within 20 min for all coatings. To address this challenge, we develop an alternative approach based on biomimicry, wherein we protect the surface from fouling using a tethered oil lubrication coating of liquid perfluorocarbon (TLP) immobilized to the surface of the microfluidic channels using a perfluorinated surface (Figure 1C).[37,39−41] The TLP surface coating, which is immiscible with a mixture of water and ethanol (Figure 1D), forms a slippery surface that suppresses fouling of the microfluidic channels during RNA-LNP formation. We employ PFD oil, a lubricant

https://doi.org/10.1021/acsnano.4c12965
ACS Nano 2025, 19, 1090−1102

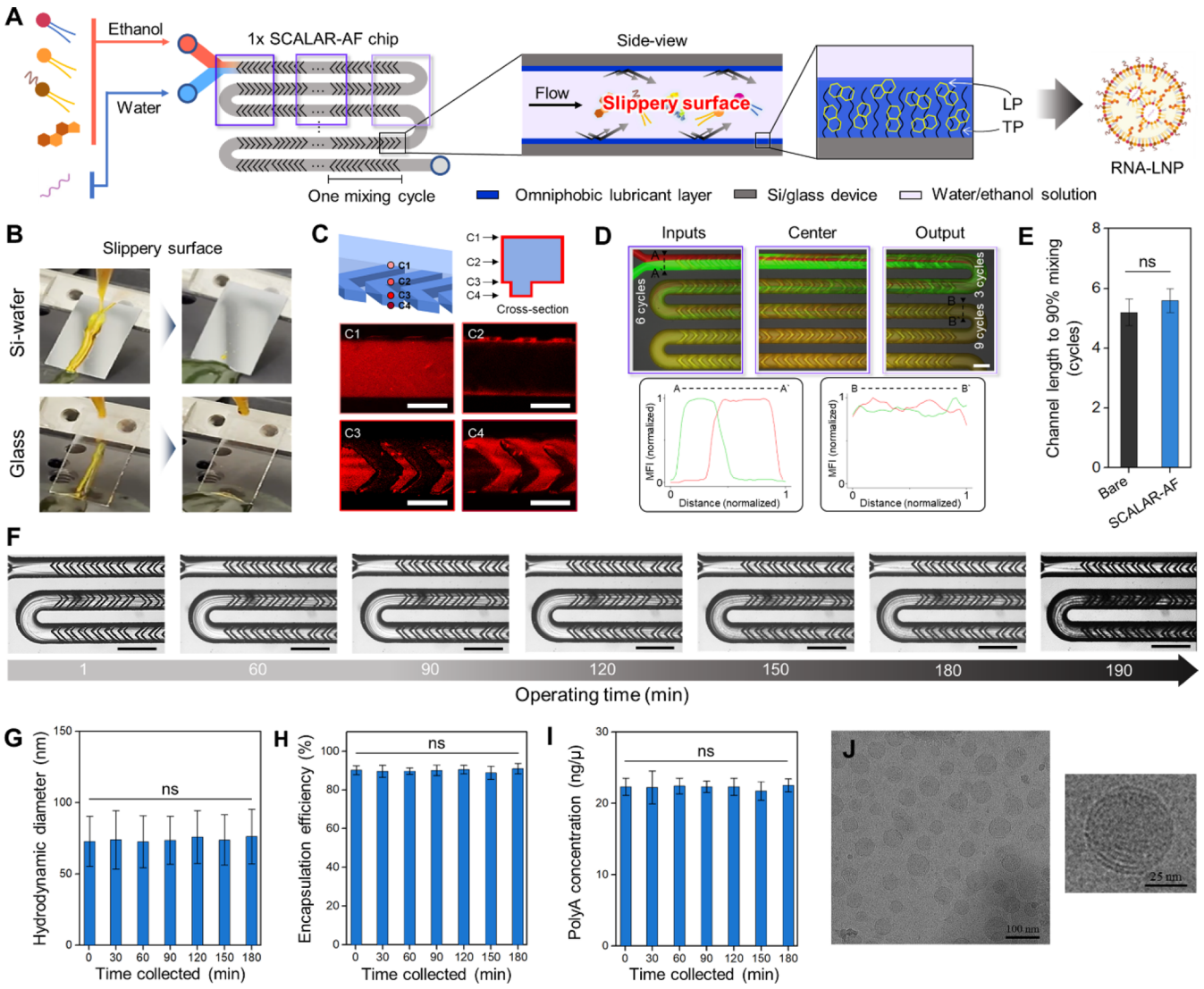

Figure 3. (A) Schematic of the production of RNA-LNP from the TLP-coated SCALAR-AF chip. (B) Photographs showing the repellency of a water/ethanol mixture (3:1) on the TLP coated Si-wafer (upper) and glass (bottom) substrates at a tilt angle of 45°. (C1−C4) Confocal micrographs showing the presence of a lubricant oil layer on the surface of the microfluidic device at different heights. (D) Micrographs revealing an excellent mixing efficiency in a 1× SCALAR-AF chip; Nile red in ethanol and FITC in water are flowed through the channel to quantify mixing at different locations along the channel; the red and green intensity profiles versus channel distance at the position of A−A′ and B−B′ (insets). Scale bar: 150 μm. (E) Quantification of mixing efficiency (±standard deviation) calculated by channel lengths required for 90% mixing for bare and 1× SCALAR-AF chip (n = 3, one-way ANOVA, ns: p > 0.05). (F) Sequential micrographs showing no severe fouling during RNA-LNP formulation over a period of ∼180 min. Scale bar: 150 μm. (G−I) Physical characterization of polyA LNPs produced by a 1× SCALAR-AF chip from 1 to 180 min. (G) Hydrodynamic diameter (±standard deviation), (H) encapsulation efficiency (±standard deviation), and (I) RNA concentration (±standard deviation) of the resulting polyA LNPs from 1 to 180 min (n = 3, one-way ANOVA, ns: p > 0.05). (J) Cryo-TEM of polyA LNPs produced by 1× SCALAR-AF chip. Scale bar: 100 and 25 nm.

oil approved by the U.S. Food and Drug Administration (FDA) for various therapeutic and biomedical applications, such as blood substitutes, cancer therapy, and diagnosis.[37,39,42] The SCALAR-AF approach successfully demonstrates continuous and robust production of RNA-LNPs for at least 3 h (>15-fold increase compared to the bare chip) without fouling (Figure 1E,F). To illustrate its applicability to scaled-up production, we design a microfluidic chip that integrates 256 parallel mixing units on a single 4 in. chip, with every generator's surface coated with TLP to prevent fouling; this chip can generate RNA-LNPs at L/h throughputs. We characterize the performance of our SCALAR-AF chip using a gold standard formulation previously optimized for siRNA and mRNA delivery, demonstrating robust LNP production. LNPs produced using SCALAR-AF chips are validated to have physiochemical properties and performance in both *in vitro* and *in vivo* model systems that matched those of uncoated chips at early time points before fouling. Beyond the LNPs generated in this article, we envision this technology finding broad utility as an antifouling lubricant layer coating in microfluidic chips for applications requiring continuous and robust production of functional particles used in drug delivery systems, cosmetic products, optical displays, pharmaceuticals, and foodstuffs. We demonstrate this potential by continuous producing of Ag_2S nanoparticles, a completely different type of nanoparticle, without any fouling in our SCALAR-AF chip.

https://doi.org/10.1021/acsnano.4c12965
ACS Nano 2025, 19, 1090−1102

RESULTS AND DISCUSSION

Evaluation of Conventional Surface Coatings to Prevent Fouling in the Microfluidic Generation of RNA-LNPs. We first evaluate the antifouling performance of various coatings that have shown antifouling properties in the literature. These coatings, some of which are hydrophobic and some of which are hydrophilic, include PEG coating (PEG-silane),[43] zwitterion coating (sulfobetaine-silane),[44,45] LbL coating (poly(acrylic acid)/polyacrylamide multilayers),[36] and fluorine coating (perfluoro-silane) (Figure 2A).[37,39−41] We confirm the modification of Si and glass surfaces with these coatings by quantifying their water contact angles in air. Upon surface modification, the water contact angles change dramatically from 37° ± 3° for Si wafer and 47° ± 4° for glass substrates to 14° ± 3°, 9° ± 3°, and 12° ± 2° upon PEG, zwitterion, and LbL coatings, respectively; these values are consistent with those reported in prior publications (Figure S2).[27−33] In contrast, the fluorine coating renders the surface hydrophobic with a contact angle value of 109° ± 5° (Figure S2). When a mixture of water and ethanol in a 3:1 volume ratio, identical to the solvent condition for RNA-LNP formulation, is placed on these surfaces that are tilted at 45°, the liquid spreads extensively and stays on the three hydrophilic surfaces (Figure 2B), indicating strong interactions between the mixture and the modified surfaces. In contrast, the perfluorosilane-treated substrate does not allow for extensive spreading of such a mixture, often resulting in pinned droplets on the tilted substrate (Figure 2B).

To test the antifouling performance of these coatings in a microfluidic mixing device used to generate RNA-LNP, we prepare a single microfluidic mixing chip on a silicon and glass (Si/glass) substrates (Figures S3 and S4) (details of these coatings on the surface of the SHM via a flow technique are as described in Experimental Section). We employ the staggered herringbone micromixer (SHM) design, characterized by short mixing times of less than 10 ms, resulting in highly uniform and small lipid nanoparticles (LNPs) (polydispersity index (PDI) <0.2 and average size <60 nm).[27,46] To evaluate our system, we use an LNP formulation that includes DLin-MC3-DMA (MC3) with phospholipid distearoylphosphatidylcholine (DSPC), cholesterol, and PEG-lipid (DMG-PEG 2000) at a molar ratio of 50:10:38.5:1.5, respectively; this composition is similar to those found in the Comirnaty and Spikevax COVID-19 mRNA vaccines developed by Pfizer/BioNTech and Moderna, respectively (Figure 2A).[4−6] PolyA is selected as a surrogate for RNA to evaluate the durability and performance of surface-modified devices owing to the high costs associated with using functional RNA. We infuse an aqueous polyA solution and an ethanolic lipid solution into each surface-modified chip with a flow rate ratio of 3:1 at a total flow rate of 1.2 mL/min by using syringe pumps or pressure driven pumps. Within 10 min of the infusion of the two solutions, we observe severe fouling in the bare Si/glass chip (Figure 2C). Dynamic light scattering (DLS) of the product stream shows that the particle size increases significantly from 70 to 200 nm in this short time span, and relatedly the uniformity of the RNA-LNPs is significantly decreased, with the PDI increasing from 0.1 to 0.5 (Figure 2C).

We next evaluate the four surface coatings described above (PEG, zwitterionic, LbL, and perfluorinated silane) to prevent fouling in the single microfluidic staggered herringbone chip. Although the surface fouling proceeds more slowly compared with the bare device, all of these coatings fail within 20 min. For all coatings, fouling becomes apparent in microscopy within 15 min of operating the device and leads to channel blockages within 20−25 min (Figure 2C). Among the four coatings, zwitterionic surface treatment provides the longest antifouling behavior; yet, the device fails in less than 20 min. As fouling progresses, the size of the produced LNPs becomes larger, exceeding 150 nm, and their size distribution becomes broader, often exhibiting a bimodal pattern. Although various hydrophilic and hydrophobic coatings are widely studied for their ability to prevent fouling, they are known for inhibiting adsorption and fouling of biomolecules in fully aqueous solutions.[42] In contrast, LNP formation involves a mixture of water and ethanol and the precipitation and self-assembly of four lipids and RNA, leading to a highly complex micro-environment that promotes the deposition of materials onto solid surfaces. Thus, commonly reported hydrophilic or hydrophobic coatings that are designed to keep water molecules tightly bound to or away from the surface are not suitable for resolving the fouling issue that arises during the LNP manufacturing process.

Continuous and Robust Manufacturing of RNA-LNPs from SCALAR-AF Chip. We next evaluated the ability of the TLP coating to prevent fouling on our chip (Figure 3A). We confirm the modification of Si and glass surfaces with TLP coatings by quantifying their water contact angle in air. The water contact angles on TLP-coated planar Si and glass substrates are 120° ± 5° and 119° ± 6°, respectively; these values are higher compared to those observed for surfaces coated with a simple perfluorosilane and are consistent with the literature (Figure S6).[37,39−41] Moreover, we observe that the TLP-coated substrates provide excellent slipperiness against the water/ethanol mixture, effectively preventing fluid retention or adhesion on the substrates (Figure 3B). To coat our chips with TLP, we (1) create reactive −OH groups on the surface by exposing the surface of the microfluidic channels and SHMs to a NaOH solution; (2) form a covalently bonded perfluorinated surface by flowing the tethered perfluorocabon (TP) silane solution through the chip, followed by heating in an oven at 60 °C for overnight; (3) apply the liquid perfluorocarbon (LP) oil layer by flowing the PFD into the chip, and (4) remove the excess PFD from the water phase by using a syringe pump (details of TLP coating on the surface of the SHM via a flow technique are as described in Experimental Section). We denote the TLP-coated microfluidic single chip as a 1 × SCALAR-AF chip. Confocal microscopy of the Rhodamine-labeled (red fluorescent dye) lubricant layer on the three dimensionally structured microfluidic channels shows conformal coating on the channel floor, ceiling, walls, and features of the SHM patterns (Figure 3C). In addition, we observe that the thickness of the lubricant layer that was formed on a planar Si wafer treated using the same protocol is 7.9 ± 0.7 nm, as measured by using an ellipsometer. Lubricant-infused coatings can change the flow characteristics of liquid above the surface and hence potentially impact the mixing efficiency of herringbone channels;[37,39] thus, we test the mixing efficiency of the 1× SCALAR-AF chip by monitoring the mixing of the aqueous and ethanolic solutions by adding fluorescein isothiocyanate (FITC) dextran and Nile red in the two solutions, respectively (Figure 3D). These two dyes are selected since they approximate the size of the lipids and RNA, respectively.[25] The mixing efficiency is evaluated by quantifying the channel length at which the two dyes are 90% mixed

https://doi.org/10.1021/acsnano.4c12965
ACS Nano 2025, 19, 1090−1102

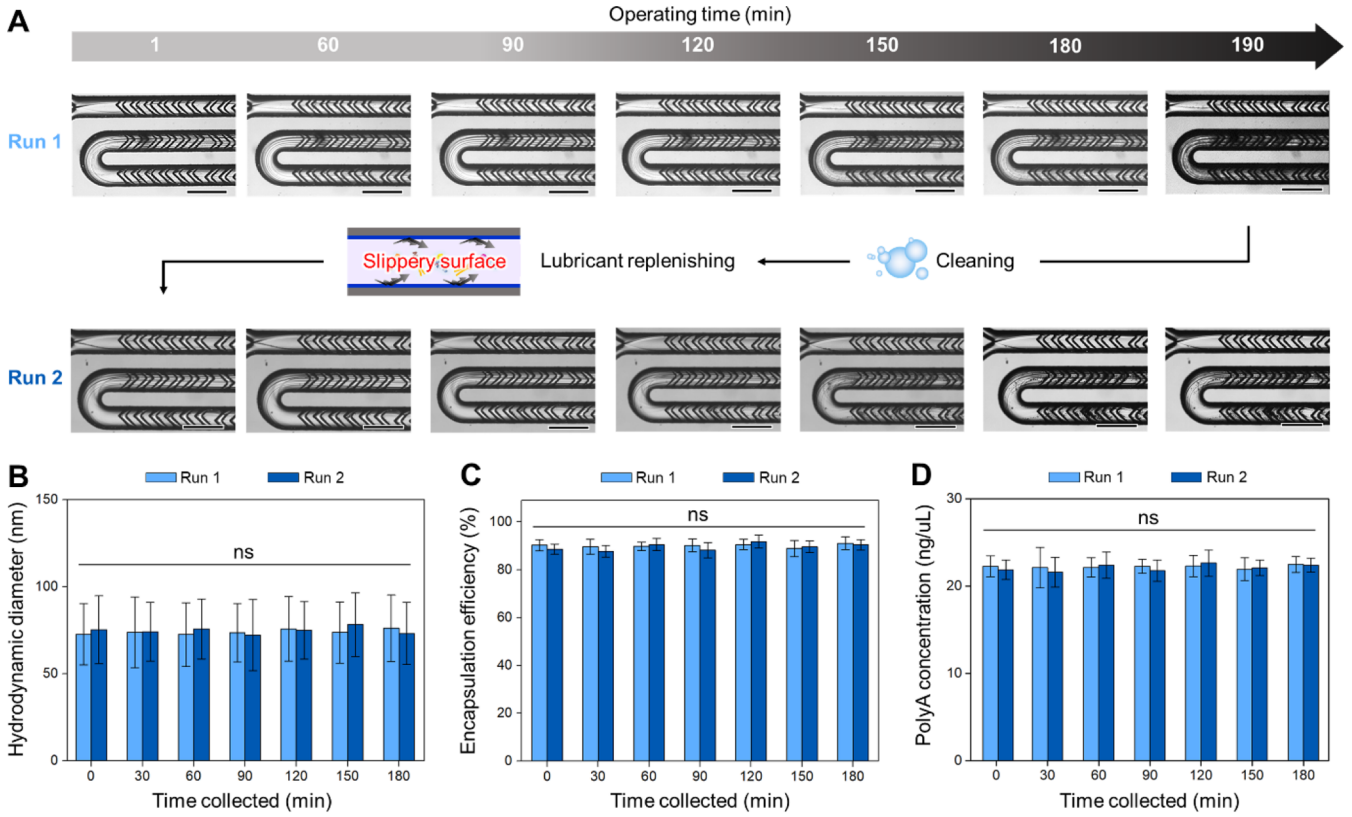

Figure 4. (A) Sequential micrographs showing no severe fouling during 2 runs of polyA LNP formulation over a period of ~180 min. Device was cleaned with 1% Triton-X 100, a nitrogen purge, and then an ethanol wash followed by a nitrogen purge again. Subsequently, perfluorodecalin (PFD) liquid was applied to create the lubricant layer for the antifouling surface. The replenished SCALAR-AF chip shows antifouling performance by repelling the multiple LNP constituents. Scale bar: 150 μm. (B–D) Physical characterization of polyA LNPs produced by a 1× SCALAR-AF chip over two successive runs. (B) Hydrodynamic diameter (±standard deviation), (C) encapsulation efficiency (±standard deviation), and (D) RNA concentration (±standard deviation) of the resulting polyA LNPs from 1 to 180 min (n = 3, one-way ANOVA, ns: p > 0.05).

(Figure 3E). At a flow rate ratio of 0.3, which is the lipid to nucleic acid ratio, the 1× SCALAR-AF chip allows excellent mixing efficiency, consistent with prior results obtained with a pristine Si/glass device.[46] The 1× SCALAR-AF chip continuously produce LNPs for at least ~180 min without severe fouling, a marked improvement over the other antifouling coatings tested which all failed within 20 min (Figure 3F). The physical characteristics of polyA LNPs show no significant changes over this time period, as evidenced by consistent hydrodynamic diameter, encapsulation efficiency, and RNA concentration throughout the 3-h period (Figure 3G-I). In addition, the cryogenic TEM images of the resulting polyA LNPs demonstrate the high uniformity of LNPs in size and morphology (Figure 3J). In addition, after using a SCALAR-AF chip for polyA LNP production for 3 h, we replenish the same chip with the lubricant oil and test its antifouling properties. The 1× SCALAR-AF chip is cleaned with 1% Triton-X 100 surfactant, a nitrogen purge, an ethanol wash, and then a nitrogen purge. Subsequently, perfluorodecalin (PFD) liquid is applied again to create the lubricant layer for the antifouling surface. The replenished SCALAR-AF chip shows the same antifouling performance as observed in the first operation (Figure 4). We find no significant differences in the hydrodynamic diameter, encapsulation efficiency, and RNA concentration (Figure 4B–D). We confirm that the replenished SCALAR-AF chip shows the antifouling performance with repeatability for robust formulation of RNA-LNP over two successive runs. To further demonstrate the versatility and broad applicability of our lubricant oil layer coating, we expand our study beyond lipid nanoparticles (LNPs) to the continuous production of inorganic Ag_2S nanoparticles. Our results show that the lubricant oil layer enables robust manufacturing of Ag_2S-NPs without any performance degradation for at least 60 min (Figure S7). In stark contrast, severe fouling occurs in a bare Si/glass chip within just 20 min, significantly compromising the process. The Ag_2S-NPs produced using our coated chip consistently maintain a diameter below 5 nm with exceptional uniformity, whereas those produced on the bare chip experience a marked increase in size and a loss of uniformity due to fouling, as clearly demonstrated in Figure S7. These compelling results reinforce our assertion that the lubricant-infused coating is highly effective not only for LNPs but also across a broad spectrum of microfluidic applications. Furthermore, to monitor the change in the amount of perfluorodecalin (PFD) in the SCALA-AF chip, we label the lubricant layer with Rhodamine and then expose it to a water/ethanol (3:1) flow at 1.2 mL/min for 20 min. Top-down fluorescent microscopy images show a minimal change in fluorescent intensity during the first 60 min. After that, the intensity gradually decreases, with a significant reduction observed at 180 min (Figure S8), indicating the depletion of the lubricant layer on the surface of the SCALAR-AF chip. We notice that the 1× SCALAR-AF chip start showing evidence of surface fouling after 3 h likely

https://doi.org/10.1021/acsnano.4c12965
ACS Nano 2025, 19, 1090–1102

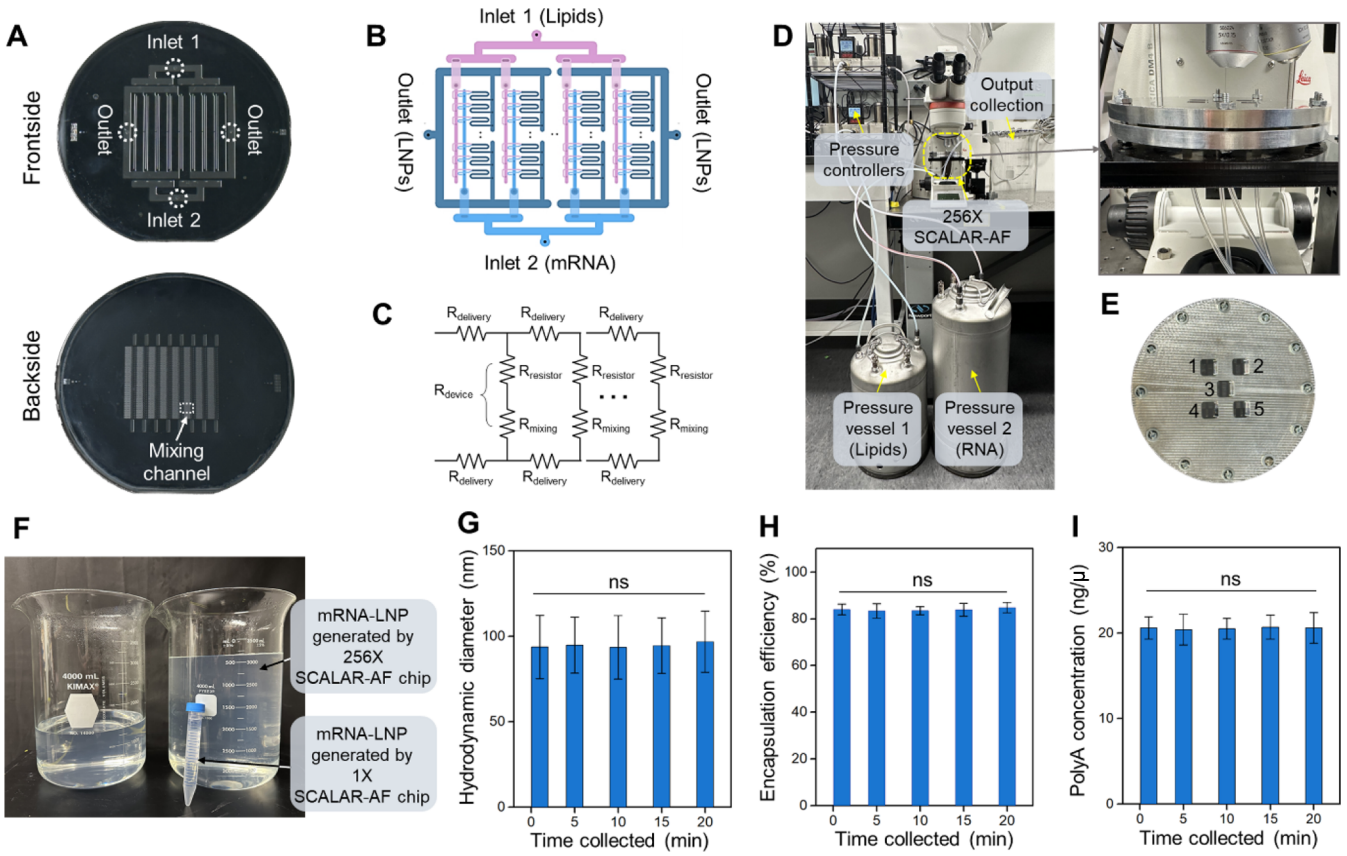

Figure 5. (A) Photographs showing the frontside (upper) and backside (bottom) views of the 256× SCALAR-AF chip. (B) Schematic of chip design illustrating the integration of branching geometry and ladder design architecture to ensure uniform distribution of inputs to each mixing unit. The schematic is not to scale. (C) Circuit model of the delivery channels ($R_{delivery}$), resistors ($R_{resistor}$), mixing channels (R_{mixing}), and individual mixing channel unit (R_{device}). (D) Photographs showing the experimental setup for scaling-up the production of RNA-LNP from the 256× SCALAR-AF chip by a custom pressure-driven flow system. (E) Photograph showing the assembled aluminum holder of the 256× SCALAR-AF chip, with the frontside windows for observation at different positions. (F) Photography image showing the relative throughput of 256× and 1× SCALAR-AF chips that produced LNPs for 20 min with resultant volumes of 4.8 L (256× chip; shown in 3.5 L beakers) and 10 min 0.012 L (1× chip; shown in a 15 mL Falcon tube), respectively. (G) Hydrodynamic diameter (±standard deviation), (H) encapsulation efficiency (±standard deviation), and (I) RNA concentration measurements (±standard deviation) of the resulting polyA LNPs produced by the 256× SCALAR-AF chip (n = 3, one-way ANOVA, ns: p > 0.05).

due to the depletion of the lubricant oil under shear as well as its diffusion into the flowing water/ethanol mixture stream.

Scaling-Up the Production of RNA-LNP via Parallelization and Surface Modification. To demonstrate the potential of this approach for industrial scale manufacturing of RNA-LNPs, we fabricate a SCALAR-AF microfluidic chip that parallelizes 256 microfluidic SHM devices (Figures 5A, S4, S5, and S9). A ladder design is applied for parallelization to distribute fluids to and collect fluids from individual mixing units (Figure 5B).[47,48] The effective resistance of a single mixing device (R_{device}), which is the sum of the resistance of a flow resistor ($R_{resistor}$) and that of the mixer (R_{mixing}), is designed to be significantly greater than the resistance of the delivery channel between two devices (Figure 5C), satisfying the previously reported design rule: $2N$ ($R_{delivery}/R_{device}$) < 0.01.[48] The TLP coating approach can be readily extended to the parallelized 256× SCALAR-AF chip thanks to the simplicity of the method as well as the uniform flow distribution that the chip design ensures. In a parallelized device, if a uniform flow distribution is compromised due to clogging, the optimal conditions for particle generation can vary across channels, potentially leading to variations in the physical properties of the resulting RNA-LNPs. Our experimental results demonstrate that the RNA-LNPs produced from this chip consistently maintain high-quality physical properties, such as hydrodynamic diameter, RNA concentration, and encapsulation efficiency, without any fouling issues. This uniformity across channels is a critical outcome of the TLP coating, which effectively prevents clogging and ensures reliable, reproducible production of RNA-LNPs.[18,25,48] In addition, we observe no considerable alteration in the flow distribution and mixing efficiency of the parallelized 256× SCALAR-AF chip (Figure S10). To validate that the 256× SCALAR-AF chip can produce LNPs at a large scale while maintaining their physical characteristics of LNPs, we produce RNA-LNPs and compare their physical properties such as hydrodynamic diameter, RNA concentration, and encapsulation efficiency with those generated using a 1× SCALAR-AF. We use C12-200, another gold-standard ionizable lipid with DSPC, cholesterol, and DMG-PEG. We use polyA as our RNA and C12-200 as the ionizable lipid (Figure S11), to make this high throughput experiment financially feasible. We inject the polyA aqueous and ethanolic lipid solutions into each input port of the 256× SCALAR-AF chip with a flow rate ratio of 3:1 at a total flow rate of 14.4 L/h using our custom-built pressure-driven flow system (Figure

https://doi.org/10.1021/acsnano.4c12965
ACS Nano 2025, 19, 1090−1102

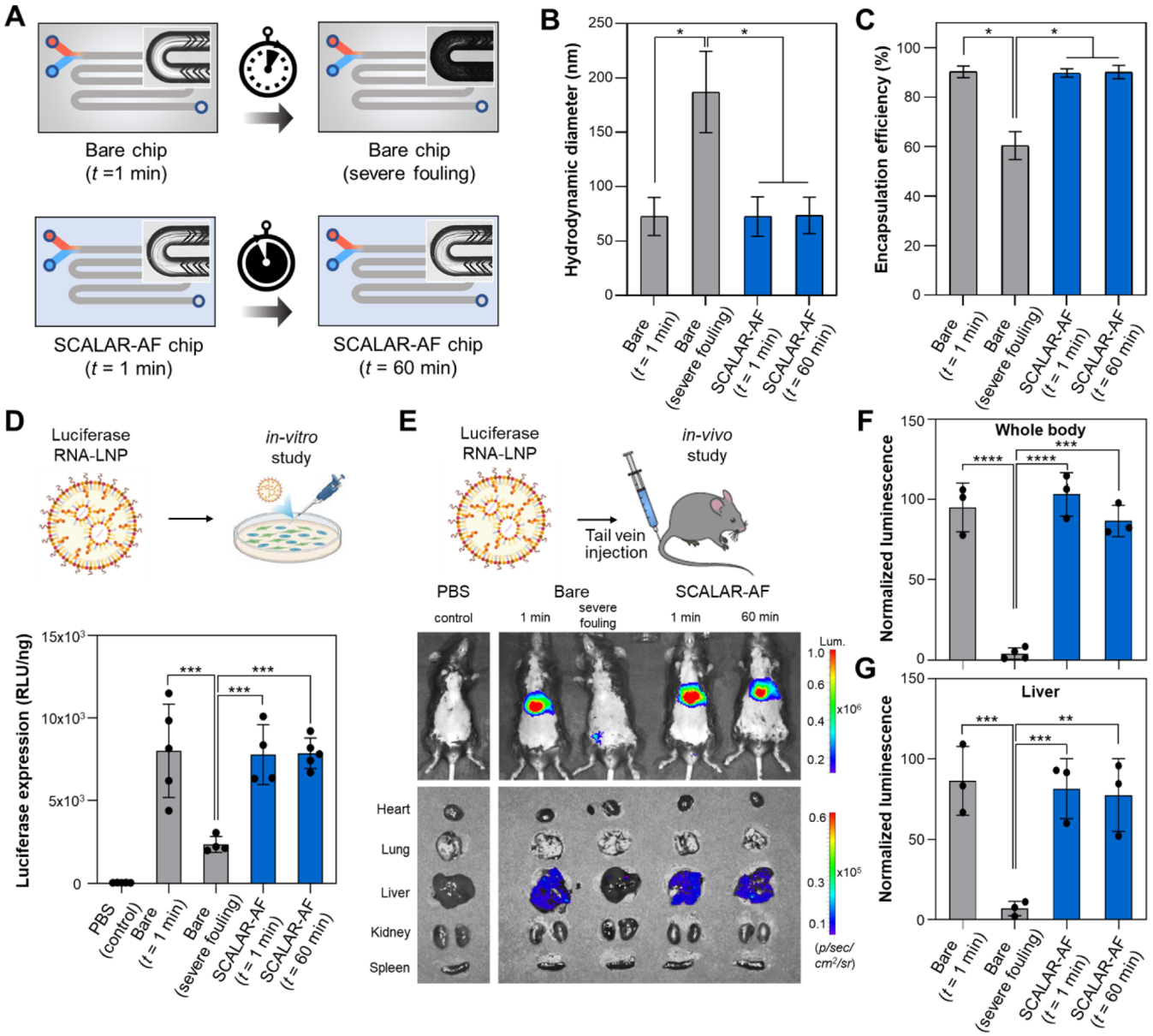

Figure 6. (A) Schematic illustration showing the luciferase RNA-LNPs generated by the bare chip (at t = 1 min and after severe fouling) and the TLP-coated SCALAR-AF chip (at t = 1 and 60 min). (B) DLS results (±standard deviation) of luciferase RNA-LNPs produced from each device. (n = 3, one-way ANOVA and Tukey's multiple comparisons, *p < 0.05). (C) RNA encapsulation efficiency (±standard deviation) from each device, quantified by a RiboGreen assay (n = 3, one-way ANOVA and Tukey's multiple comparisons, *p < 0.05). (D) Luciferase RNA-LNPs are formulated and administered to HeLa cells at a dose of 60 ng/60,000 cells; luciferase expression is quantified by luminescence after 6 h (n = 4−5, one-way ANOVA and Tukey's multiple comparisons, ***p < 0.001). (E) Luciferase RNA-LNPs are formulated and administered to mice via tail vein injection at a dose of 4 μg per mouse. Representative IVIS imaging at 6 h after LNP administration, showing luciferase expression in the whole body (upper) and dissected organs (bottom). (F) Quantification of luciferase signal in the whole body at 6 h after LNP administration (n = 3−4, one-way ANOVA and Tukey's multiple comparisons, ***p < 0.001; ****p < 0.0001). (G) Quantification of luciferase signal in the liver (n = 3, one-way ANOVA and Tukey's multiple comparisons, **p < 0.01; ***p < 0.001).

5D). The chip is able to produce polyA LNPs for 20 min without fouling with a resultant volume of 4.8 L, which is equivalent to 2.4 g of RNA or 9,600 vaccine doses (Figure 5F). Additionally, we confirm that the LNP hydrodynamic diameter (~80 nm), encapsulation efficiency (>80%), and the RNA concentration (~22.5 ng/μL) measured during the 20 min operation of the parallelized chip are comparable to those measured for resulting formulation from the 1× SCALAR-AF chip (Figure 5G−I). The cost to fabricate our chip at the university of Pennsylvania is approximately $2,000 per 4″ wafer. This cost can be greatly reduced as scale-up production is increased. Moreover, this expense is only a fraction of the overall cost of producing high-quality LNPs, given that the price of critical reagents (e.g., lipids and RNA) is exceptionally high, with mRNA costing more than $2,000 per 1 mg.

In Vitro and In Vivo Validation of RNA LNPs Prepared from SCALAR-AF Chip. We evaluated the potential impact of TLP-coating on the potency of RNA LNPs. To this end, we use the TLP-coated SCALAR-AF to formulate luciferase RNA-LNPs and compare their physical properties as well as their *in*

https://doi.org/10.1021/acsnano.4c12965
ACS Nano 2025, 19, 1090−1102

vitro and *in vivo* activity to LNPs generated by a bare chip (t = 1 min and after severe fouling) (Figure 6A). We encapsulate mRNA encoding luciferase in LNPs composed of MC3, a well-validated ionizable lipid that has been FDA approved for RNA delivery, phospholipid DSPC, cholesterol, and lipid-anchored PEG (DMG-PEG 2000) at a molar ratio of 50:10:38.5:1.5. While the LNPs generated by bare chips after severe fouling have a dramatic increase in their size (>150 nm) and size heterogeneity (PDI > 0.4); in contrast, LNPs generated by the 1× SCALAR-AF chip at t = 1 and 60 min show no significant changes in the hydrodynamic size (<80 nm) and size distribution (PDI < 0.2) (Figure 6B). In addition, encapsulation efficiency measurements, quantified by a Ribo-Green assay, demonstrate that the 1× SCALAR-AF chip maintains a high encapsulation efficiency (>85%) after 60 min, whereas the encapsulation efficiency of the bare chip degrades significantly to ∼60% over the same period of time (Figure 6C).

For *in vitro* evaluation, HeLa cells are selected to demonstrate a potential application for cell engineering (i.e., gene delivery) using RNA-LNPs (Figure 6D). We deliver luciferase-encoding RNA-LNPs to HeLa cells at doses of 60 ng of RNA per 60k cells. We observe that while the luciferase expression of luciferase RNA-LNPs formulated by 1× SCALAR-AF chip at t = 1 and 60 min show high activity, the potency of LNPs produced by a bare chip after severe fouling degrades by 4-fold compared to LNPs produced at t = 1 min (Figure 6D). For *in vivo* testing, these RNA-LNPs are administered to C57BL/6 mice via tail vein injection at 4 μg per mouse, and we quantify the luminescent signal in the whole body and dissected major organs (i.e., heart, spleen, liver, lung, and kidneys) after 6 h (Figure 6E). We observe that there are no significant differences between the whole-body and liver luminescent signals for RNA- LNPs prepared using the 1× SCALAR-AF chip at both t = 1 and 60 min (Figure 6F,G). Although RNA-LNPs produced from the bare chip at t = 1 min show a strong luminescent signal, the potency of the LNPs degrades dramatically to the point where little luminescence is detected in the whole-body and in the liver when the device is fouled and clogged (Figure 6F,G). The poor performance of the LNPs produced from bare chips after fouling is likely due to the larger LNP size (>150 nm) as well as lower encapsulation efficiency (∼60%), leading to rapid blood clearance by the reticuloendothelial system and restricted traversal through liver fenestrations.[11,15,49] Overall, these results demonstrate that our antifouling TLP chip can formulate highly potent RNA-LNPs for potential applications of RNA therapeutics and vaccines.

CONCLUSIONS

We present a promising solution to the persistent challenge of fouling in microfluidic mixing devices for RNA-LNP production. By making use of recent work on using immobilized liquid lubricant layers to avoid fouling in complex solutions,[37,39−41] we have successfully created an antifouling surface capable of repelling the diverse constituents of LNPs in the mixture of solvents used in their production. This approach, applied to a SHM mixing chip, extends stable operation to over 3 h, representing a substantial improvement over the conventional method. Furthermore, our approach is scalable, as demonstrated by its compatibility with a parallelized microfluidic platform incorporating 256 SHM mixers, achieving production rates suitable for commercial applications. Importantly, we confirm that LNPs produced using our coated chip maintain identical physicochemical properties and performance for both *in vitro* and *in vivo* RNA delivery, compared to uncoated devices at short time-scales before they foul, validating the efficacy of our antifouling strategy in maintaining LNP quality.

This advancement holds significant promise for advancing microfluidic LNP production toward broader adoption in commercial manufacturing, enabling enhanced precision and reliability in RNA-based therapeutics and vaccine development. While our work has demonstrated promising results and a significant step forward in the field of microfluidic LNP production for RNA-based therapeutics, there are still challenges to overcome. For example, we believe that by adjusting the viscosity of the liquid lubricant layer and optimizing channel design, we can extend device lifetime further.[40,50−54] We anticipate that these efforts will contribute to the continued advancement of microfluidic technology for LNP production and may have broader implications for nanomedicine, medical device, and microparticles synthesis via continuous-flow lithography, by establishing a low-adhesion nonfouling interface. This coating technology presents a major breakthrough, ensuring robust, continuous production of functional nanoparticles, which are critical in fields such as drug delivery, electronics, catalysis, optical displays, and foodstuffs. By effectively mitigating fouling, our approach significantly enhances the scalability and reliability of microfluidic manufacturing, positioning it as a versatile solution for diverse industrial applications.

EXPERIMENTAL SECTION

Chip Fabrication. In the case of a single 1× chip, the process involved omitting the delivery channel (layer 1) while keeping all other procedures identical. The chips were fabricated at the Quattrone Nanofabrication Facility, University of Pennsylvania. The chip design comprised four mask layers designed in AutoCAD (Autodesk, San Rafael, CA), defining the delivery channels (layer 1), mixing channels (layer 2), herringbones and resistors (layer 3), and through silicon vias (etching layer 4; layer 5 overall) (Figure S4). Chrome-coated soda lime photomasks (AZ1500; Telic Company, Santa Clarita, CA) were patterned using a Heidelberg laser writer with a 10 mm write head and developed in an AZ 300MIF developer (EMD Performance Materials Corp., Philadelphia, PA). Chromium was etched with Transene chromium etchant (Danvers, MA), and the photoresist was removed with Remover 1165 (DuPont, Wilmington, DE). Fabrication proceeded by lithographically patterning each layer on 100 mm silicon wafers (ID 775; University Wafer, South Boston, MA), followed by deep reactive ion etching (DRIE). For lithography, a S1805 photoresist (Dow, Midland, MI) was spray-coated to the desired thickness using an AS8 Alta Spray Coater (SUSS MicroTec, Garching, Germany).

First etching layer: the wafer was dipped in 49% hydrofluoric acid (HF), spray-coated with 16 μm of photoresist, and soft-baked at 110 °C for 10 min. The delivery channel design was exposed using a MA6 mask aligner (SUSS MicroTec), baked at 110 °C for 5 min, developed in an AZ 300MIF developer, rinsed with water, dried with N_2, and baked at 110 °C for 10 min. The wafer was etched to a 370 μm depth using DRIE (SPTS Rapier Si DRIE, Newport, UK), cleaned using acetone and isopropanol (IPA) for 5 min each, then cleaned by immersion in Nano-Strip (CMC Materials, Aurora, IL), followed by cleaning in a Spin Rinse Dryer (SRD; RENA Compass, RENA, Albany, OR).

Second etching layer: after 49% HF dipping, the wafer's backside was coated with 8 μm of photoresist, baked at 110 °C for 5 min, and exposed with the mixing channel design. Then, the wafer was developed and baked at 110 °C for 5 min. DRIE was used to etch the

https://doi.org/10.1021/acsnano.4c12965
ACS Nano 2025, 19, 1090−1102

material to a 70 μm depth. The wafer was then cleaned using acetone, IPA, Nano-Strip, and SRD as before.

Third etching layer: the wafer was dipped in 49% HF, then the backside of the wafer was coated with 4 μm of photoresist and baked in an oven at 110 °C for 5 min, then developed and baked in an oven at 110 °C for 5 min, and etched to a 25 μm etch depth using DRIE. Plasma-enhanced chemical vapor deposition (Oxford Plasma Lab 100 PECVD) (Oxford Instruments, Abingdon, UK) deposited 4 μm of SiO_2, followed by cleaning using Nano-Strip and SRD.

Fourth etching layer: the frontside of the wafer was coated with 8 μm of photoresist, baked at 110 °C for 5 min, and exposed to the through silicon via design. The wafer was developed, baked at 110 °C for 5 min, and then etched to a 60 μm depth using DRIE. Cleaning steps included acetone, IPA, and 25% HF for 5 min.

After etching, the silicon wafer and a 100 mm Borofloat 33 glass wafer (ID 517; University Wafer) were cleaned using Nano-Strip and SRD as before. Another Borofloat 33 glass wafer was micromachined with 1 mm holes for the inlets and outlets. Then this wafer was cleaned using Nano-Strip and SRD. For a single 1× chip, a glass wafer was anodically bonded on one side of the Si wafer. For a 256× chip, two glass wafers were anodically bonded to either side of the silicon wafer using an EVG 510 Wafer Bonding System (EVG Group, Oberosterreich, Austria) at 900 V with 1000 N for 1 h. We note that these Si/glass chips demonstrate high pressure resistance (P_{max} > 1000 psi (pounds per square inch)) and high temperature (T_{max} > 500 °C) tolerance, along with excellent solvent resistance, making them ideal microfluidic platforms for large-scale nanomaterial manufacturing.[48]

Surface Coating Methods. Basically, to coat our chips with TLP, the Si/glass microfluidic mixing chip was flushed by infusing a 0.01 M NaOH solution to activate the hydroxyl group (−OH) on the surface of Si/glass microchannels for 30 min at room temperature, followed by rinsing with water and ethanol. Then, we formed a covalently bonded tethered perfluorocarbon (TP) surface by flowing the liquid silane solution (5%v/v trichloro(1*H*,1*H*,2*H*,2*H*-perfluorooctyl)silane (Sigma-Aldrich) in anhydrous ethanol (Sigma-Aldrich)) for 6 h at room temperature. The chip was rinsed with anhydrous ethanol and gently heated in an oven with desiccant at 60 °C overnight. We applied the liquid perfluorocarbon (LP) oil layer into the channel by flowing perfluorodecalin (PFD, Sigma-Aldrich) oil, followed by removing excess PFD with the water phase by using a syringe pump at the flow rate of 1 mL/h. In addition, the thickness of the lubricant layer on a planar Si wafer was measured by using an ellipsometer (Alpha-SE, J.A. Woollam Co., Inc., USA).

For different coatings, some of which are hydrophobic and some of which are hydrophilic, include PEG coating (PEG-silane),[43] zwitterion coating (sulfobetaine-silane),[44,45] LbL coating (poly(acrylic acid)/polyacrylamide multilayers),[36] and fluorine coating (perfluorosilane)[37,39−41] These coating methods were prepared based on methods reported in prior papers and using flow surface coating methods.

For PEG coating, we formed a covalently bonded PEG surface by flowing a liquid silane solution (15 wt % mPEG-silane (M_n 5 000, Sigma-Aldrich) in anhydrous dimethyl sulfoxide (DMSO, Sigma-Aldrich)) for 1 h at 90 °C, followed by rinsing with anhydrous DMSO.

For zwitterion coating, we formed a covalently bonded zwitterion surface by flowing a liquid sulfobetaine silane solution (10 mM SBSi (3-(dimethyl(3-trimethoxysilyl)propyl)ammonium propane-1-sulfonate, Gelest) in pH 3.5 DI water) for 6 h at room temperature, followed by rinsing with pH 3 DI water.

For LbL coating, we formed the LbL assembly of multilayer films by alternately flowing a liquid 10 mM solutions of poly(acrylic acid) (PAA, M_w ∼ 50 000, 25% aqueous solution, Sigma-Aldrich) and polyacrylamide (PAAm, M_w ∼ 5 000 000−6 000 000, Sigma-Aldrich) in pH 3 DI water. For 10 bilayers of a PAA/PAAm film inside a microfluidic chip, the PAA solution and the PAAm solution were applied sequentially for 10 min each, with a 2 min rinsing step in pH 3 deionized water performed between the two polymer adsorption processes. After LbL assembly, the PAA/PAAm was cross-linked in a vacuum oven for 8 h at 180 °C.

For fluorine coating, we formed a covalently bonded fluorine surface by flowing the liquid silane solution (5%v/v trichloro-(1*H*,1*H*,2*H*,2*H*-perfluorooctyl)silane (Sigma-Aldrich) in anhydrous ethanol (Sigma-Aldrich)) for 6 h at room temperature, followed by rinsing with anhydrous ethanol.

Lipid Synthesis. The synthesis of the ionizable lipid C12-200 was achieved by combining *N*1-(2-(4-(2-aminoethyl)piperazin-1-yl)-ethyl)ethane-1,2-diamine (1.00 g, 4.64 mmol, 1.0 equiv), ethanol (10 mL), and 1,2-epoxydodecane (7.10 mL, 32.5 mmol, 7.0 equiv) in a 50 mL round-bottom flask equipped with a stir bar. The reaction mixture was maintained at 80 °C for 48 h under constant stirring. Subsequently, ethanol was removed under reduced pressure and the residue was diluted with 15 mL of dichloromethane (DCM). Purification of the crude product was performed using a Teledyne ISCO CombiFlash system with a 40 g RediSep Gold silica gel column, employing a gradient elution from 100% DCM to a mixture of 20% DCM and 80% Ultra solution over 30 min. The process was carried out in two separate runs, each utilizing half of the DCM solution. The resulting C12-200 was collected as a yellow-orange oil with a 37% yield and analyzed by ^{1}H NMR spectroscopy (Figure S11). ^{1}H NMR spectra were obtained on a Bruker NEO 400 MHz spectrometer using deuterated chloroform ($CDCl_3$) as the solvent. ^{1}H NMR (400 MHz, $CDCl_3$) δ: 4.99−3.30 (m, 8H), 3.14−1.99 (m, 30H), 1.84−1.05 (m, 90H), 1.05−0.67 (m, 15H).

RNA-LNPs Formulation Using 1× and 256× SCALAR-AF Chips. RNA-loaded lipid nanoparticles (RNA-LNPs) were prepared through either microfluidic mixing or pipet-based rapid mixing of an aqueous RNA solution with an ethanol-based lipid mixture. The aqueous phase included luciferase RNA (TriLink) or polyA (Roche) at a concentration of 24.7 μg/mL in a 10 mM citrate buffer (Alpha Teknova, Inc., Hollister, CA). The ethanol phase contained D-Lin-MC3-DMA (MedChemExpress, Monmouth Junction, NJ), DSPC (1,2-distearoyl-*sn*-glycero-3-phosphocholine; Avanti Polar Lipids, Alabaster, AL), cholesterol (Sigma-Aldrich, St. Louis, MO), and DMG-PEG 2000 (Avanti Polar Lipids), mixed in ethanol at molar ratios of 50%, 10%, 38.5%, and 1.5%, respectively. All formulations maintained a 10:1 weight ratio of ionizable lipid to RNA, yielding a final RNA-LNP concentration of 271.7 μg/mL. The aqueous and ethanol phases were combined at a 3:1 flow rate ratio with a total volumetric flow rate of 1.2 mL/min using syringe pumps or a custom-built pressure-driven flow system. For large-scale RNA-LNP production, the synthesized ionizable lipid C12-200 was used instead of MC3. The aqueous phase contained polyA RNA at 24.7 μg/mL in 10 mM citrate buffer, while the ethanol phase included C12-200, DSPC, cholesterol, and DMG-PEG 2000 in molar ratios of 50%, 10%, 38.5%, and 1.5%, respectively. A custom-built pressure driven flow system (Figure 4D) rated to 100 pounds per square inch (psi) delivered fluids to the chip. The 10:1 lipid-to-RNA weight ratio was maintained. A nitrogen tank connected to dual-valve pressure controllers (Alicat Scientific, Tucson, AZ), operated via FlowVision 2.0 software, regulated the fluid flow to the microfluidic chip. These pressure controllers directed RNA and lipid solutions from stainless steel pressure vessels (5-gallon for RNA, 3-gallon for lipids; Alloy Products Corp., Waukesha, WI) through PTFE tubing (1/4″ OD, McMaster-Carr, Elmhurst, IL). Downstream connections to the chip employed 1/4 in. OD PTFE and 1/8 in. OD FEP tubing (McMaster-Carr). The system, mounted on an xyz translational stage (Figure S6), allowed performance monitoring during operation. LNPs were subsequently dialyzed against 1× PBS using 20 kDa MWCO dialysis cassettes (Thermo Fisher, Waltham, MA) for 4 h.

Characterization of RNA-LNPs. Lipid nanoparticles (LNPs) were characterized using dynamic light scattering (DLS) on a DynaPro Plate Reader III (Wyatt Technology, Santa Barbara, CA) to determine the hydrodynamic diameter and polydispersity index (PDI). The reported sizes represent intensity-weighted averages, and the standard deviation of the particle size was calculated using the formula: $\sigma = (\text{PDI} \times \text{diameter}^2)^{1/2}$. RNA concentrations were quantified through A260 absorbance measurements performed with a

https://doi.org/10.1021/acsnano.4c12965
ACS Nano 2025, 19, 1090−1102

Tecan NanoQuant Plate (Thermo Fisher) and an Infinite M Plex plate reader (Tecan, Männedorf, Switzerland). Relative encapsulation efficiency was assessed using the RiboGreen Quant-iT RNA assay kit (Thermo Fisher), following the manufacturer's protocol, and expressed as the percentage of RNA encapsulated relative to the total RNA in the sample. For cryo-EM analysis, 3 μL of LNPs at an approximate RNA concentration of 100 ng/μL was applied to glow-discharged Quantifoil holey carbon grids. The grids were blotted and plunge-frozen in liquid ethane using a Vitrobot Mark IV (Thermo Scientific). Imaging was conducted at the Beckman Center for Cryo-EM with a Titan Krios (Thermo Scientific) equipped with a K3 BioQuantum detector.

RNA Delivery Studies In Vitro. Firefly luciferase-expressing HeLa cells were cultured in Dulbecco's Modified Eagle's Medium (DMEM) (Thermo Fisher), supplemented with 10% fetal bovine serum (FBS) and 1% penicillin/streptomycin, and maintained at 37 °C with 5% CO_2. Cells were counted, mixed at a 1:1 ratio, and seeded at a density of 10,000 cells per well in a 96-well plate (Thermo Fisher). After plating, the cells were treated with luciferase RNA-LNPs, and luminescence was measured 6 h post-treatment using the Luciferase Assay System (Promega), following the manufacturer's instructions. Luminescent signals were normalized to untreated cells after subtracting background luminescence from the control wells containing only reagents without cells. Cytotoxicity was evaluated using the Cell Titer-Glo Luminescent Cell Viability Assay (Promega), performed according to the manufacturer's protocol. The resulting luminescence values were normalized to those of untreated cells after accounting for background luminescence.

Animal Studies. Animal experiments were conducted using 6–8-week-old female C57BL/6 mice (The Jackson Laboratory) in compliance with protocols approved by the Institutional Animal Care and Use Committee (IACUC) at the University of Pennsylvania. For the luciferase study, mice received intramuscular injections of luciferase RNA-LNPs at a dose of 4 μg of RNA per mouse. Six hours after administration, the mice were injected intraperitoneally with D-luciferin potassium salt at a dose of 150 mg/kg. Whole-body and major organ bioluminescence imaging was conducted by using an in vivo imaging system (IVIS; PerkinElmer, Waltham, MA). Bioluminescence signals were quantified by calculating the photon flux in defined regions of interest using Living Image 4.7.3 software (PerkinElmer), with photon flux values normalized to the image background.

Statistical Information. Statistical analyses were conducted using GraphPad Prism 9. Results are expressed as the mean ± standard deviation unless stated otherwise. Comparisons between two groups were performed using one-way analysis of variance (ANOVA), while Tukey's post hoc test was applied for multiple group comparisons. $p < 0.05$ was considered statistically significant.

Continuous Production of Ag_2S Nanoparticles. Two solutions were prepared and coinjected by syringe pumps into each bare and SCALA-AF chip, which were prepared as previously described. One solution was prepared with 767 mg of L-glutathione (GSH, 98%, Sigma-Aldrich) and 42.5 mg of $AgNO_3$ (99%, Sigma-Aldrich) in 75 mL of DI water, then the pH of this solution was adjusted to 7.4 using NaOH (Fisher Scientific). Then, for the second solution, 10 mg of Na_2S (Sigma-Aldrich) was dissolved in 25 mL of DI water. The two solutions were simultaneously injected into each bare and SCALA-AF chip at a 3:1 flow rate ratio, respectively, with a total flow rate of 1.2 mL/min. The products were collected, concentrated, and subsequently washed with deionized (DI) water using 3 kDa molecular weight cutoff (MWCO) filtration tubes (Sartorius Stedim Biotech, Germany). Filtration was carried out by centrifugation at 4000 rpm for 20 min. The concentrated nanoparticles were further purified by passing them through a 0.02 μm filter membrane (Whatman Anotop, Boston, MA). The samples were analyzed using a cryo-electron microscope. ImageJ software was used to measure the core diameter of the nanoparticles. 100 nanoparticles per sample were analyzed.

ASSOCIATED CONTENT

Data Availability Statement

The authors declare that the data supporting the findings of this study are included in the article and/or the Supporting Information files.

Supporting Information

The Supporting Information is available free of charge at https://pubs.acs.org/doi/10.1021/acsnano.4c12965.

Manufacturing of mRNA LNPs using PDMS device; the contact angle analysis of water in air on Si-wafer and glass substrates with various coatings; an aluminum holder customized for the 1× and 256× SCALAR-AF chip; the fabrication process for the Si/glass microfluidic chip; the dimension information on the microfluidic chip; top-down views of the SCALAR-AF chip with the Rhodamine-labeled lubricant perfluorodecalin layer; fluorescent mixing images; and ^{1}H NMR characterization of C12-200 ionizable lipid (Figures S1–S11) (PDF)

AUTHOR INFORMATION

Corresponding Authors

David A. Issadore − *Department of Chemical and Biomolecular Engineering and Department of Bioengineering, University of Pennsylvania, Philadelphia, Pennsylvania 19104, United States; Department of Electrical and Systems Engineering, University of Pennsylvania, Philadelphia, Pennsylvania 19104, United States;* orcid.org/0000-0002-5461-8653; Email: issadore@seas.upenn.edu

Daeyeon Lee − *Department of Chemical and Biomolecular Engineering, University of Pennsylvania, Philadelphia, Pennsylvania 19104, United States;* orcid.org/0000-0001-6679-290X; Email: daeyeon@seas.upenn.edu

Authors

Yoon-Ho Hwang − *Department of Chemical and Biomolecular Engineering, University of Pennsylvania, Philadelphia, Pennsylvania 19104, United States; Department of Polymer Engineering, Pukyong National University, Nam-gu, Busan 48513, Republic of Korea*

Sarah J. Shepherd − *Department of Bioengineering, University of Pennsylvania, Philadelphia, Pennsylvania 19104, United States*

Dongyoon Kim − *Department of Bioengineering, University of Pennsylvania, Philadelphia, Pennsylvania 19104, United States;* orcid.org/0000-0002-1769-6505

Alvin J. Mukalel − *Department of Bioengineering, University of Pennsylvania, Philadelphia, Pennsylvania 19104, United States*

Michael J. Mitchell − *Department of Bioengineering, University of Pennsylvania, Philadelphia, Pennsylvania 19104, United States; Department of Medicine, Institute for Immunology, Perelman School of Medicine, Cardiovascular Institute, Perelman School of Medicine, Institute for Regenerative Medicine, Perelman School of Medicine, Abramson Cancer Center, Perelman School of Medicine, Penn Institute for RNA Innovation, Perelman School of Medicine, and Department of Electrical and Systems Engineering, University of Pennsylvania, Philadelphia, Pennsylvania 19104, United States;* orcid.org/0000-0002-3628-2244

Complete contact information is available at: https://pubs.acs.org/10.1021/acsnano.4c12965

https://doi.org/10.1021/acsnano.4c12965
ACS Nano 2025, 19, 1090−1102

Notes

The authors declare the following competing financial interest(s): Daeyeon Lee and David Issadore are the co-founders of InfiniFluidics.

ACKNOWLEDGMENTS

We acknowledge the support from the Wellcome Leap R3 program. Y.-H.H. acknowledges the support from the Sejong Science Fellowship of the National Research Foundation (NRF) of Korea grant funded by the Korean government (No. RS-2023-00254042). We thank Phillip Iaccarino for his help with confocal analysis. We also thank the staff of the Singh Center for Nanotechnology at the University of Pennsylvania for their help with Si/glass device fabrication.

REFERENCES

(1) Pardi, N.; Hogan, M. J.; Porter, F. W.; Weissman, D. mRNA vaccines - a new era in vaccinology. *Nat. Rev. Drug Discovery* **2018**, *17* (4), 261−279.
(2) Pardi, N.; Hogan, M. J.; Weissman, D. Recent advances in mRNA vaccine technology. *Curr. Opin. Immunol.* **2020**, *65*, 14−20.
(3) Reichmuth, A. M.; Oberli, M. A.; Jaklenec, A.; Langer, R.; Blankschtein, D. mRNA vaccine delivery using lipid nanoparticles. *Ther. Deliv.* **2016**, *7* (5), 319−334.
(4) Milane, L.; Amiji, M. Clinical approval of nanotechnology-based SARS-CoV-2 mRNA vaccines: impact on translational nanomedicine. *Drug Delivery Transl. Res.* **2021**, *11* (4), 1309−1315.
(5) Polack, F. P.; Thomas, S. J.; Kitchin, N.; Absalon, J.; Gurtman, A.; Lockhart, S.; Perez, J. L.; Pérez Marc, G.; Moreira, E. D.; Zerbini, C. Safety and Efficacy of the BNT162b2 mRNA COVID-19 Vaccine. *N. Engl. J. Med.* **2020**, *383* (27), 2603−2615.
(6) Baden, L. R.; El Sahly, H. M.; Essink, B.; Kotloff, K.; Frey, S.; Novak, R.; Diemert, D.; Spector, S. A.; Rouphael, N.; Creech, C. B. Efficacy and Safety of the mRNA-1273 SARS-CoV-2 Vaccine. *N. Engl. J. Med.* **2021**, *384* (5), 403−416.
(7) Semple, S. C.; Leone, R.; Barbosa, C. J.; Tam, Y. K.; Lin, P. J. C. Lipid Nanoparticle Delivery Systems to Enable mRNA-Based Therapeutics. *Pharmaceutics* **2022**, *14* (2), 398.
(8) Mehta, M.; Bui, T. A.; Yang, X.; Aksoy, Y.; Goldys, E. M.; Deng, W. Lipid-Based Nanoparticles for Drug/Gene Delivery: An Overview of the Production Techniques and Difficulties Encountered in Their Industrial Development. *ACS Mater. Au* **2023**, *3* (6), 600−619.
(9) Guevara, M. L.; Persano, F.; Persano, S. Advances in Lipid Nanoparticles for mRNA-Based Cancer Immunotherapy. *Front. Chem.* **2020**, *8*, 589959.
(10) Kulkarni, J. A.; Cullis, P. R.; van der Meel, R. Lipid Nanoparticles Enabling Gene Therapies: From Concepts to Clinical Utility. *Nucleic Acid Ther.* **2018**, *28* (3), 146−157.
(11) Hou, X.; Zaks, T.; Langer, R.; Dong, Y. Lipid nanoparticles for mRNA delivery. *Nat. Rev. Mater.* **2021**, *6* (12), 1078−1094.
(12) Mulligan, M. J.; Lyke, K. E.; Kitchin, N.; Absalon, J.; Gurtman, A.; Lockhart, S.; Neuzil, K.; Raabe, V.; Bailey, R.; Swanson, K. A. Phase I/II study of COVID-19 RNA vaccine BNT162b1 in adults. *Nature* **2020**, *586* (7830), 589−593.
(13) Kowalski, P. S.; Rudra, A.; Miao, L.; Anderson, D. G. Delivering the Messenger: Advances in Technologies for Therapeutic mRNA Delivery. *Mol. Ther.* **2019**, *27* (4), 710−728.
(14) Jung, H. N.; Lee, S. Y.; Lee, S.; Youn, H.; Im, H. J. Lipid nanoparticles for delivery of RNA therapeutics: Current status and the role of in vivo imaging. *Theranostics* **2022**, *12* (17), 7509−7531.
(15) Hassett, K. J.; Benenato, K. E.; Jacquinet, E.; Lee, A.; Woods, A.; Yuzhakov, O.; Himansu, S.; Deterling, J.; Geilich, B. M.; Ketova, T. Optimization of Lipid Nanoparticles for Intramuscular Administration of mRNA Vaccines. *Mol. Ther. Nucleic Acids* **2019**, *15*, 1−11.
(16) Nakamura, T.; Kawai, M.; Sato, Y.; Maeki, M.; Tokeshi, M.; Harashima, H. The Effect of Size and Charge of Lipid Nanoparticles Prepared by Microfluidic Mixing on Their Lymph Node Transitivity and Distribution. *Mol. Pharmaceutics* **2020**, *17* (3), 944−953.
(17) Hashiba, A.; Toyooka, M.; Sato, Y.; Maeki, M.; Tokeshi, M.; Harashima, H. The use of design of experiments with multiple responses to determine optimal formulations for in vivo hepatic mRNA delivery. *J. Controlled Release* **2020**, *327*, 467−476.
(18) Shepherd, S. J.; Warzecha, C. C.; Yadavali, S.; El-Mayta, R.; Alameh, M.-G.; Wang, L.; Weissman, D.; Wilson, J. M.; Issadore, D.; Mitchell, M. J. Scalable mRNA and siRNA Lipid Nanoparticle Production Using a Parallelized Microfluidic Device. *Nano Lett.* **2021**, *21* (13), 5671−5680.
(19) Webb, C.; Forbes, N.; Roces, C. B.; Anderluzzi, G.; Lou, G.; Abraham, S.; Ingalls, L.; Marshall, K.; Leaver, T. J.; Watts, J. A. Using microfluidics for scalable manufacturing of nanomedicines from bench to GMP: A case study using protein-loaded liposomes. *Int. J. Pharm.* **2020**, *582*, 119266.
(20) Jahn, A.; Stavis, S. M.; Hong, J. S.; Vreeland, W. N.; DeVoe, D. L.; Gaitan, M. Microfluidic Mixing and the Formation of Nanoscale Lipid Vesicles. *ACS Nano* **2010**, *4* (4), 2077−2087.
(21) Liu, Y.; Yang, G.; Hui, Y.; Ranaweera, S.; Zhao, C.-X. Microfluidic Nanoparticles for Drug Delivery. *Small* **2022**, *18* (36), 2106580.
(22) Ma, Z.; Li, B.; Peng, J.; Gao, D. Recent Development of Drug Delivery Systems through Microfluidics: From Synthesis to Evaluation. *Pharmaceutics* **2022**, *14* (2), 434.
(23) Maeki, M.; Uno, S.; Niwa, A.; Okada, Y.; Tokeshi, M. Microfluidic technologies and devices for lipid nanoparticle-based RNA delivery. *J. Controlled Release* **2022**, *344*, 80−96.
(24) Shepherd, S. J.; Issadore, D.; Mitchell, M. J. Microfluidic formulation of nanoparticles for biomedical applications. *Biomater* **2021**, *274*, 120826.
(25) Shepherd, S. J.; Han, X.; Mukalel, A. J.; El-Mayta, R.; Thatte, A. S.; Wu, J.; Padilla, M. S.; Alameh, M.-G.; Srikumar, N.; Lee, D.; Weissman, D. Throughput-scalable manufacturing of SARS-CoV-2 mRNA lipid nanoparticle vaccines. *Proc. Nat. Acad. Sci.* **2023**, *120* (33), No. e2303567120.
(26) Hwang, Y.-H.; Um, T.; Ahn, G.-N.; Kim, D.-P.; Lee, H. Robust and scalable production of emulsion-templated microparticles in 3D-printed milli-fluidic device. *Chem. Eng. J.* **2022**, *431*, 133998.
(27) Seo, H.; Jeon, L.; Kwon, J.; Lee, H. High-Precision Synthesis of RNA-Loaded Lipid Nanoparticles for Biomedical Applications. *Adv. Health. Mater.* **2023**, *12* (13), 2203033.
(28) Cho, W. K.; Kong, B.; Choi, I. S. Highly Efficient Non-Biofouling Coating of Zwitterionic Polymers: Poly((3-(methacryloylamino)propyl)-dimethyl(3-sulfopropyl)ammonium hydroxide). *Langmuir* **2007**, *23* (10), 5678−5682.
(29) Massenburg, S. S.; Amstad, E.; Weitz, D. A. Clogging in parallelized tapered microfluidic channels. *Microfluid. Nanofluid* **2016**, *20*, 94.
(30) Wang, Z.; Voicu, D.; Tang, L.; Li, W.; Kumacheva, E. Microfluidic studies of polymer adsorption in flow. *Lab Chip* **2015**, *15* (9), 2110−2116.
(31) Schoenitz, M.; Grundemann, L.; Augustin, W.; Scholl, S. Fouling in microstructured devices: a review. *Chem. Commun.* **2015**, *51* (39), 8213−8228.
(32) Lowe, S.; O'Brien-Simpson, N. M.; Connal, L. A. Antibiofouling polymer interfaces: poly(ethylene glycol) and other promising candidates. *Poly. Chem.* **2015**, *6* (2), 198−212.
(33) Hu, J.; Zhang, H.; Sun, B.; Lu, A.; Zhong, G.; Chen, Z. Integration of antifouling and foul-release moieties for optimizing the performance of PEG-silicone coatings. *J. Coat. Technol. Res.* **2021**, *18* (6), 1669−1677.
(34) Skinner, M.; Johnston, B. M.; Liu, Y.; Hammer, B.; Selhorst, R.; Xenidou, I.; Perry, S. L.; Emrick, T. Synthesis of Zwitterionic Pluronic Analogs. *Biomacromol* **2018**, *19* (8), 3377−3389.
(35) Abraham, M. H.; Acree, W. E., Jr Solvation Descriptors for Zwitterionic α-Aminoacids; Estimation of Water−Solvent Partition Coefficients, Solubilities, and Hydrogen-Bond Acidity and Hydrogen-Bond Basicity. *ACS Omega* **2019**, *4* (2), 2883−2892.

https://doi.org/10.1021/acsnano.4c12965
ACS Nano 2025, 19, 1090−1102

(36) Lee, S.-W.; Tettey, K. E.; Kim, I. L.; Burdick, J. A.; Lee, D. Controlling the Cell-Adhesion Properties of Poly(acrylic acid)/Polyacrylamide Hydrogen-Bonded Multilayers. *Macromol* **2012**, *45* (15), 6120−6126.
(37) Leslie, D. C.; Waterhouse, A.; Berthet, J. B.; Valentin, T. M.; Watters, A. L.; Jain, A.; Kim, P.; Hatton, B. D.; Nedder, A.; Donovan, K. A bioinspired omniphobic surface coating on medical devices prevents thrombosis and biofouling. *Nat. Biotechnol.* **2014**, *32* (11), 1134−1140.
(38) Wang, X.-T.; Deng, X.; Zhang, T.-D.; Zhang, J.; Chen, L.-L.; Wang, Y.-F.; Cao, X.; Zhang, Y.-Z.; Zheng, X.; Yin, D.-C. A Versatile Hydrophilic and Antifouling Coating Based on Dopamine Modified Four-Arm Polyethylene Glycol by One-Step Synthesis Method. *ACS Macro Lett.* **2022**, *11* (6), 805−812.
(39) Epstein, A. K.; Wong, T.-S.; Belisle, R. A.; Boggs, E. M.; Aizenberg, J. Liquid-infused structured surfaces with exceptional anti-biofouling performance. *Proc. Natl. Acad. Sci.* **2012**, *109* (33), 13182−13187.
(40) MacCallum, N.; Howell, C.; Kim, P.; Sun, D.; Friedlander, R.; Ranisau, J.; Ahanotu, O.; Lin, J. J.; Vena, A.; Hatton, B. Liquid-Infused Silicone As a Biofouling-Free Medical Material. *ACS Biomater. Sci. Eng.* **2015**, *1* (1), 43−51.
(41) Howell, C.; Grinthal, A.; Sunny, S.; Aizenberg, M.; Aizenberg, J. Designing Liquid-Infused Surfaces for Medical Applications: A Review. *Adv. Mater.* **2018**, *30* (50), 1802724.
(42) Douglass, M.; Garren, M.; Devine, R.; Mondal, A.; Handa, H. Bio-inspired hemocompatible surface modifications for biomedical applications. *Prog. Mater. Sci.* **2022**, *130*, 100997.
(43) Gidi, Y.; Bayram, S.; Ablenas, C. J.; Blum, A. S.; Cosa, G. Efficient One-Step PEG-Silane Passivation of Glass Surfaces for Single-Molecule Fluorescence Studies. *ACS Appl. Mater. Interfaces* **2018**, *10* (46), 39505−39511.
(44) Estephan, Z. G.; Jaber, J. A.; Schlenoff, J. B. Zwitterion-Stabilized Silica Nanoparticles: Toward Nonstick Nano. *Langmuir* **2010**, *26* (22), 16884−16889.
(45) Estephan, Z. G.; Hariri, H. H.; Schlenoff, J. B. One-pot, exchange-free, room-temperature synthesis of sub-10 nm aqueous, noninteracting, and stable zwitterated iron oxide nanoparticles. *Langmuir* **2013**, *29* (8), 2572−2579.
(46) Stroock, A. D.; Dertinger, S. K.; Ajdari, A.; Mezic, I.; Stone, H. A.; Whitesides, G. M. Chaotic mixer for microchannels. *Science* **2002**, *295* (5555), 647−651.
(47) Romanowsky, M. B.; Abate, A. R.; Rotem, A.; Holtze, C.; Weitz, D. A. High throughput production of single core double emulsions in a parallelized microfluidic device. *Lab Chip* **2012**, *12* (4), 802−807.
(48) Yadavali, S.; Jeong, H.-H.; Lee, D.; Issadore, D. Silicon and glass very large scale microfluidic droplet integration for terascale generation of polymer microparticles. *Nat. Commun.* **2018**, *9* (1), 1222.
(49) Swingle, K. L.; Hamilton, A. G.; Mitchell, M. J. Lipid Nanoparticle-Mediated Delivery of mRNA Therapeutics and Vaccines. *Trends Mol. Med.* **2021**, *27* (6), 616−617.
(50) Howell, C.; Vu, T. L.; Johnson, C. P.; Hou, X.; Ahanotu, O.; Alvarenga, J.; Leslie, D. C.; Uzun, O.; Waterhouse, A.; Kim, P. Stability of Surface-Immobilized Lubricant Interfaces under Flow. *Chem. Mater.* **2015**, *27* (5), 1792−1800.
(51) Kolle, S.; Ahanotu, O.; Meeks, A.; Stafslien, S.; Kreder, M.; Vanderwal, L.; Cohen, L.; Waltz, G.; Lim, C. S.; Slocum, D.; Greene, E. M. On the mechanism of marine fouling-prevention performance of oil-containing silicone elastomers. *Sci. Rep.* **2022**, *12* (1), 11799.
(52) Ozkan, E.; Mondal, A.; Douglass, M.; Hopkins, S. P.; Garren, M.; Devine, R.; Pandey, R.; Manuel, J.; Singha, P.; Warnock, J. Bioinspired ultra-low fouling coatings on medical devices to prevent device-associated infections and thrombosis. *J. Colloid Interface Sci.* **2022**, *608*, 1015−1024.
(53) Roberts, T. R.; Choi, J. H.; Wendorff, D. S.; Harea, G. T.; Beely, B. M.; Sieck, K. N.; Douglass, M. E.; Singha, P.; Dean, J. B.; Handa, H.; Batchinsky, A. I. Tethered Liquid Perfluorocarbon Coating for 72 h Heparin-Free Extracorporeal Life Support. *Asaio J.* **2021**, *67* (7), 798−808.
(54) Sunny, S.; Vogel, N.; Howell, C.; Vu, T. L.; Aizenberg, J. Lubricant-Infused Nanoparticulate Coatings Assembled by Layer-by-Layer Deposition. *Adv. Funct. Mater.* **2014**, *24* (42), 6658−6667.

https://doi.org/10.1021/acsnano.4c12965
ACS Nano 2025, 19, 1090−1102